

Correlation between the strength of low-temperature T-linear normal-state resistivity and T_c in overdoped electron-doped cuprate superconductors

Xingyu Ma¹, Minghuan Zeng¹, Huaiming Guo², and Shiping Feng^{1*}
¹*Department of Physics, Beijing Normal University, Beijing 100875, China and*
²*School of Physics, Beihang University, Beijing 100191, China*

The recently observed an intimate link between the nature of the strange metallic normal-state and superconductivity in the overdoped electron-doped cuprate superconductors is calling for an explanation. Here the intrinsic correlation between the strength of the low-temperature linear-in-temperature normal-state resistivity and superconducting transition temperature T_c in the overdoped electron-doped cuprate superconductors is studied within the framework of the kinetic-energy-driven superconductivity. On the one hand, the main ingredient is identified into a electron pairing mechanism involving *the spin excitation*, and then T_c has a dome-like shape doping dependence with the maximal T_c that occurs at around the optimal electron doping. On the other hand, in the normal-state above T_c , the low-temperature linear-in-temperature normal-state resistivity in the overdoped regime arises from the momentum relaxation due to the electron umklapp scattering mediated by *the same spin excitation*. This *same spin excitation* that governs both the electron umklapp scattering responsible for the low-temperature linear-in-temperature normal-state resistivity and electron pairing responsible for superconductivity naturally generates a correlation between the strength of the low-temperature linear-in-temperature normal-state resistivity and T_c in the overdoped regime.

PACS numbers: 74.25.Fy, 74.25.Nf, 74.20.Mn, 74.72.-h

I. INTRODUCTION

The undoped parent compounds of cuprate superconductors are antiferromagnetic (AF) Mott insulators¹, which result from the particularly strong electron correlation². However, the exceptionally strong superconductivity can be achieved when the AF long-range order (AFLRO) is destroyed by a small fraction of the electron or hole doping concentration^{3,4}. In particular, although both the electron doping and annealing process in a low-oxygen environment are required to induce superconductivity in the electron-doped cuprate superconductors⁵⁻⁷, the experimental observations demonstrate unambiguously that in a proper annealing condition, the superconducting (SC) phase is extended over a wide electron doping range with the SC transition temperature T_c that reaches its maximum at around the optimal electron doping $\delta \sim 0.15$, while the disappearance of AFLRO at the doping is coincident with the onset of superconductivity, and hence the deduced AFLRO phase boundary does not extend into the SC dome⁸⁻¹¹. This phase diagram of the electron-doped cuprate superconductors bears striking similarity to the corresponding phase diagram in the hole-doped counterparts¹², providing an experimental evidence for the absence of the disparity between the phase diagrams of the electron- and hole-doped cuprate superconductors. This absence of the disparity between the phase diagrams⁸⁻¹¹ also suggests that the essential physics, including the SC mechanism and the nature of the normal-state, is most likely the same for both the electron- and hole-doped cuprate superconductors.

After intensive investigations over thirty years, a substantial amount of reliable and reproducible data for the

electron-doped cuprate superconductors has been accumulated through systematic measurements using various techniques¹³⁻²³, which indicate that the normal-state property of these materials is a remarkable mystery and the most important unsolved problem in condensed matter physics. In particular, the normal-state property¹⁷⁻²³ in the overdoped regime deviates from the conventional Fermi-liquid behavior²⁴⁻²⁶. This has led to the normal-state in the overdoped regime being referred to as *the strange metallic normal-state*²⁷⁻²⁹. One of the key manifestations of this deviation is the low-temperature linear-in-temperature (T-linear) resistivity, which persists down to millikelvin temperatures and extrapolates to zero resistivity at zero temperature¹⁷⁻²³. Recently, this low-temperature T-linear normal-state resistivity in the overdoped electron-doped cuprate superconductors has been confirmed experimentally all the way up to the edge of the SC dome²³. More importantly, these experimental observations also establish definitively that in the overdoped regime, the low-temperature T-linear normal-state resistivity is tied to T_c , where the strength of the low-temperature T-linear normal-state resistivity (then the T-linear normal-state resistivity coefficient) follows a scaling relation with the corresponding magnitude of T_c , and then the strength of the low-temperature T-linear normal-state resistivity decreases as T_c decreases. This surprising correlation between the strength of the low-temperature T-linear normal-state resistivity and the corresponding magnitude of T_c in the overdoped electron-doped cuprate superconductors²³ therefore strongly suggests an intimate link between the nature of the strange metallic normal-state and superconductivity. In other words, the origin of the strange metallic normal-state is intertwined with the origin of superconductivity. In

this case, the strange metallic normal-state of the overdoped electron-doped cuprate superconductors potentially serves as a starting point for a deep understanding of the SC mechanism of cuprate superconductivity.

Although the intrinsic correlation between the strength of the low-temperature T-linear normal-state resistivity and the corresponding magnitude of T_c in the overdoped electron-doped cuprate superconductors has been established experimentally^{19–23}, a complete understanding of this correlation is still unclear, where a key question is whether a common bosonic excitation, which dominates both the electron scattering responsible for the low-temperature T-linear normal-state resistivity and the electron pairing responsible for superconductivity, makes a correlation between the strength of the low-temperature T-linear normal-state resistivity and the corresponding magnitude of T_c . In the recent work³⁰, the doping-temperature phase diagram in the electron-doped cuprate superconductors was discussed based on the kinetic-energy-driven SC mechanism, where the main ingredient is identified into the constrained electron pairing mechanism involving *the spin excitation, the collective mode from the internal spin degree of freedom of the constrained electron itself*, and then the obtained T_c increases with the increase of electron doping in the underdoped regime, and reaches its maximum in the optimal electron doping, then decreases in the overdoped regime. On the other hand, the nature of the low-temperature T-linear normal-state resistivity in the overdoped hole-doped cuprate superconductors was investigated very recently³¹, where the origin of the low-temperature T-linear normal-state resistivity is attributed to the electron umklapp scattering from the spin excitation. In particular, a very low temperature T_{scale} scales with Δ_p^2 , where Δ_p is the minimal umklapp vector at the antinode, and then above T_{scale} , the normal-state resistivity is T-linear with the strength that decreases with the increase of hole doping. In this paper, we study the remarkable correlation between the strength of the low-temperature T-linear normal-state resistivity and the corresponding magnitude of T_c in the overdoped electron-doped cuprate superconductors along with these lines, where we identify explicitly that the momentum relaxation due to the electron umklapp scattering mediated by the spin excitation reveals itself in the nature of the low-temperature T-linear normal-state resistivity in the overdoped electron-doped cuprate superconductors as it works in the overdoped hole-doped counterparts³¹. Our results in this paper together with the previous work for superconductivity³⁰ therefore indicate that the *spin excitation* is at the origin of both the low-temperature T-linear normal-state resistivity and superconductivity in the overdoped electron-doped cuprate superconductors. This *same spin excitation* that mediates both the electron umklapp scattering responsible for the low-temperature T-linear normal-state resistivity in the overdoped regime and attractive interaction between the electrons responsible for superconductivity naturally generates a striking

correlation between the strength of the low-temperature T-linear normal-state resistivity and the corresponding magnitude of T_c in the overdoped electron-doped cuprate superconductors.

This paper is organized as follows. The theoretical framework is presented in Sec. II, where a brief review of the doping-temperature phase diagram of the electron-doped cuprate superconductors is given for the convenience in the discussions of the correlation between the strength of the low-temperature T-linear normal-state resistivity and the corresponding magnitude of T_c in the overdoped electron-doped cuprate superconductors. The transport scattering rate, however, is obtained in terms of the spin-excitation-mediated electron umklapp scattering, and is used to derive the normal-state resistivity within the framework of the Boltzmann transport theory. The quantitative characteristics of the correlation between the strength of the low-temperature T-linear normal-state resistivity and the corresponding magnitude of T_c in the overdoped regime are presented in Section III, where it is shown that as in the hole-doped case³¹, the normal-state resistivity in the overdoped electron-doped cuprate superconductors also exhibits a crossover from the T-linear behaviour in the low-temperature region into the quadratic in temperature (T-quadratic) behaviour in the far lower temperature region. Finally, we give a summary in Sec. IV.

II. THEORETICAL FORMALISM

A. Model and electron local constraint

The basic element of the crystal structure of both the electron- and hole-doped cuprate superconductors is the square-lattice copper-oxide plane in which superconductivity occurs upon either electron or hole doping^{3,4}. As in the hole-doped case², the various signature features of the electron-doped cuprate superconductors can be also properly captured by the t - J model on a square lattice,

$$H = -t \sum_{\langle ll' \rangle \sigma} C_{l\sigma}^\dagger C_{l'\sigma} + t' \sum_{\langle\langle ll' \rangle\rangle \sigma} C_{l\sigma}^\dagger C_{l'\sigma} + \mu \sum_{l\sigma} C_{l\sigma}^\dagger C_{l\sigma} + J \sum_{\langle ll' \rangle} \mathbf{S}_l \cdot \mathbf{S}_{l'}, \quad (1)$$

where $C_{l\sigma}^\dagger$ ($C_{l\sigma}$) creates (annihilates) an electron with spin σ (either \uparrow or \downarrow) on site l , \mathbf{S}_l is a localized spin operator with its components S_l^x , S_l^y , and S_l^z , while the chemical potential μ fixes the total number of electrons. The angle brackets $\langle ll' \rangle$ and $\langle\langle ll' \rangle\rangle$ indicate the summations over the nearest-neighbor (NN) and next NN pairs, respectively, the NN hopping amplitude $t < 0$ and next NN hoping amplitude $t' < 0$ for the electron-doped case, while $t > 0$ and $t' > 0$ in the hole-doped side. Moreover, it has been shown that although the NN hopping amplitude t in the t - J model (1) has a electron-hole symmetry since the sign of t can be absorbed by the

change of the sign of the orbital on one sublattice, the electron-hole asymmetry can be properly considered by the next NN hopping amplitude^{32–34} t' . Throughout this paper, the NN magnetic exchange coupling J is set as the energy unit, and t and t' are set to $t/J = -2.5$ and $t'/t = 0.3$, respectively, as in the previous discussions of the low-energy electronic structure of the electron-doped cuprate superconductors³⁰. However, to compare with the experimental energy scales, we set $J = 1000\text{K}$.

This t - J model (1) is the strong coupling limit of the Hubbard model, and then the crucial difficulty of its solution lies in enforcing the electron on-site local constraint^{35–38}, i.e., this t - J model (1) is subject to a on-site local constraint of no double electron occupancy in the hole-doped case: $\sum_{\sigma} C_{l\sigma}^{\dagger} C_{l\sigma} \leq 1$, while it is subject a on-site local constraint of no zero electron occupancy in the electron-doped side: $\sum_{\sigma} C_{l\sigma}^{\dagger} C_{l\sigma} \geq 1$. In the hole-doped case, the fermion-spin transformation^{39,40} has been developed, where the on-site local constraint of no double electron occupancy can be treated properly in the actual analyses. To apply this fermion-spin transformation^{39,40} to the electron-doped case, the t - J model (1) in the electron representation can be converted into the t - J model in the hole representation by virtue of a particle-hole transformation $C_{l\sigma} \rightarrow f_{l-\sigma}^{\dagger}$ as³⁰,

$$H = t \sum_{\langle ll' \rangle \sigma} f_{l\sigma}^{\dagger} f_{l'\sigma} - t' \sum_{\langle\langle ll' \rangle\rangle \sigma} f_{l\sigma}^{\dagger} f_{l'\sigma} - \mu \sum_{l\sigma} f_{l\sigma}^{\dagger} f_{l\sigma} + J \sum_{\langle ll' \rangle} \mathbf{S}_l \cdot \mathbf{S}_{l'}, \quad (2)$$

and then the on-site local constraint of no zero electron occupancy in the electron representation $\sum_{\sigma} C_{l\sigma}^{\dagger} C_{l\sigma} \geq 1$ is transformed into the on-site local constraint of no double hole occupancy in the hole representation $\sum_{\sigma} f_{l\sigma}^{\dagger} f_{l\sigma} \leq 1$, where $f_{l\sigma}^{\dagger}$ ($f_{l\sigma}$) is the creation (annihilation) operator for a hole on site l with spin σ . In this case, the t - J model (1) in both the electron- and hole-doped cases is always subject to a on-site local constraint that double occupancy of a site by two fermions of opposite spins is not allowed, while the difference between the electron doping and hole doping is reflected in the sign difference of the hopping integrals as we have mentioned above. The physics of the no double occupancy in the fermion-spin transformation^{39,40} is taken into account by representing the fermion operator $f_{l\sigma}$ as a composite object created by,

$$f_{l\uparrow} = a_{l\uparrow}^{\dagger} S_l^{-}, \quad f_{l\downarrow} = a_{l\downarrow}^{\dagger} S_l^{+}, \quad (3)$$

and then the on-site local constraint of no double occupancy is satisfied in actual analyses, where the $U(1)$ gauge invariant spinful fermion operator $a_{l\sigma}^{\dagger} = e^{i\Phi_{l\sigma}} a_l^{\dagger}$ ($a_{l\sigma} = e^{-i\Phi_{l\sigma}} a_l$) creates (annihilates) a charge carrier on site l , and therefore keeps track of the charge degree of freedom of the constrained electron together with some effects of spin configuration rearrangements due to the presence of the doped electron itself, while the $U(1)$ gauge

invariant spin operator S_l^{+} (S_l^{-}) keeps track of the spin degree of freedom of the constrained electron, and therefore the collective mode from this spin degree of freedom of the constrained electron can be interpreted as the spin excitation responsible for the dynamical spin response of the system. In this fermion-spin representation (3), the t - J model (2) can be expressed as,

$$H = -t \sum_{\langle ll' \rangle} (a_{l\uparrow}^{\dagger} a_{l'\uparrow} S_{l'}^{+} S_l^{-} + a_{l\downarrow}^{\dagger} a_{l'\downarrow} S_{l'}^{-} S_l^{+}) + t' \sum_{\langle\langle ll' \rangle\rangle} (a_{l\uparrow}^{\dagger} a_{l'\uparrow} S_{l'}^{+} S_l^{-} + a_{l\downarrow}^{\dagger} a_{l'\downarrow} S_{l'}^{-} S_l^{+}) + \mu \sum_{l\sigma} a_{l\sigma}^{\dagger} a_{l\sigma} + J_{\text{eff}} \sum_{\langle ll' \rangle} \mathbf{S}_l \cdot \mathbf{S}_{l'}, \quad (4)$$

with $J_{\text{eff}} = (1 - \delta)^2 J$, and the doping concentration $\delta = \langle a_{l\sigma}^{\dagger} a_{l\sigma} \rangle = \langle a_l^{\dagger} a_l \rangle$. As in the hole-doped case³¹, the kinetic-energy term in the t - J model (4) in the fermion-spin representation has been transformed into the strong coupling between charge and spin degrees of freedom of the constrained electron, and thus governs the essential physics in the electron-doped cuprate superconductors.

B. Kinetic-energy-driven superconductivity

In the early days of superconductivity research, the kinetic-energy-driven SC mechanism for the hole-doped cuprate superconductors^{40–43} was established based on the t - J model in the fermion-spin representation, where the spin-excitation-mediated attractive interaction, which pairs the charge carriers together to form the d-wave charge-carrier pairing state, arises directly from the coupling of the charge and spin degrees of freedom of the constrained electron in the kinetic energy of the t - J model, while the electron pairs with the d-wave symmetry are generated from this d-wave charge-carrier pairing state in terms of the charge-spin recombination⁴³, and then the condensation of these electron pairs reveals the d-wave SC ground-state. This kinetic-energy-driven SC mechanism reveals that (i) the constrained electron has dual roles, since the glue to hold the constrained electron pairs together is *the spin excitation, the collective mode from the spin degree of freedom of the constrained electron itself*. In other words, the constrained electrons simultaneously act to glue and to be glued^{44,45}; (ii) the spin-excitation-mediated electron pairing state in a way is in turn strongly influenced by the single-particle coherence, leading to a dome-like shape doping dependence of T_c . Starting from the t - J model (4) in the fermion-spin representation, the formalism of the kinetic-energy-driven superconductivity developed for the hole-doped case has been generalized to the electron-doped side^{30,46}, where the complicated line-shape in the energy distribution curve, the kink in the electron dispersion, and the autocorrelation of the angle-resolved photoemission spectroscopy have been discussed, and the obtained

results are well consistent with the corresponding experimental results^{8–11}. Our following discussions of the correlation between the strength of the low-temperature T-linear normal-state resistivity and the corresponding magnitude of T_c in the overdoped electron-doped cuprate superconductors builds on the kinetic-energy-driven SC mechanism, and only a short summary of the formalism is therefore given. In the previous discussions^{30,46}, the self-consistent Dyson's equations for the hole diagonal and off-diagonal propagators of the t - J model (4) in the fermion-spin representation have been obtained in terms of the Eliashberg's approach⁴⁷ as,

$$G_f(\mathbf{k}, \omega) = G_f^{(0)}(\mathbf{k}, \omega) + G_f^{(0)}(\mathbf{k}, \omega)[\Sigma_{\text{ph}}^{(f)}(\mathbf{k}, \omega)G_f(\mathbf{k}, \omega) - \Sigma_{\text{pp}}^{(f)}(\mathbf{k}, -\omega)\mathfrak{S}_f^\dagger(\mathbf{k}, \omega)], \quad (5a)$$

$$\mathfrak{S}_f^\dagger(\mathbf{k}, \omega) = G_f^{(0)}(\mathbf{k}, -\omega)[\Sigma_{\text{ph}}^{(f)}(\mathbf{k}, -\omega)\mathfrak{S}_f^\dagger(\mathbf{k}, -\omega) + \Sigma_{\text{pp}}^{(f)}(\mathbf{k}, -\omega)G_f(\mathbf{k}, \omega)], \quad (5b)$$

where $G_f^{(0)-1}(\mathbf{k}, \omega) = \omega - \varepsilon_{\mathbf{k}}^{(f)}$ is the hole non-interacting (diagonal) propagator of the t - J model (2), with the non-interaction band energy $\varepsilon_{\mathbf{k}}^{(f)} = -4t\gamma_{\mathbf{k}} + 4t'\gamma'_{\mathbf{k}} + \mu$, $\gamma_{\mathbf{k}} = (\cos k_x + \cos k_y)/2$, and $\gamma'_{\mathbf{k}} = \cos k_x \cos k_y$, and then the full hole diagonal and off-diagonal propagators $G_f(\mathbf{k}, \omega)$ and $\mathfrak{S}_f^\dagger(\mathbf{k}, \omega)$ can be derived directly from the above Dyson's equations as,

$$G_f(\mathbf{k}, \omega) = \frac{1}{\omega - \varepsilon_{\mathbf{k}}^{(f)} - \Sigma_{\text{tot}}^{(f)}(\mathbf{k}, \omega)}, \quad (6a)$$

$$\mathfrak{S}_f^\dagger(\mathbf{k}, \omega) = \frac{L^{(f)}(\mathbf{k}, \omega)}{\omega - \varepsilon_{\mathbf{k}}^{(f)} - \Sigma_{\text{tot}}^{(f)}(\mathbf{k}, \omega)}, \quad (6b)$$

with the functions,

$$\Sigma_{\text{tot}}^{(f)}(\mathbf{k}, \omega) = \Sigma_{\text{ph}}^{(f)}(\mathbf{k}, \omega) + \frac{|\Sigma_{\text{pp}}^{(f)}(\mathbf{k}, \omega)|^2}{\omega + \varepsilon_{\mathbf{k}}^{(f)} + \Sigma_{\text{ph}}^{(f)}(\mathbf{k}, -\omega)}, \quad (7a)$$

$$L^{(f)}(\mathbf{k}, \omega) = -\frac{\Sigma_{\text{pp}}^{(f)}(\mathbf{k}, \omega)}{\omega + \varepsilon_{\mathbf{k}}^{(f)} + \Sigma_{\text{ph}}^{(f)}(\mathbf{k}, -\omega)}, \quad (7b)$$

where the hole normal self-energy $\Sigma_{\text{ph}}^{(f)}(\mathbf{k}, \omega)$ in the particle-hole channel and the hole anomalous self-energy $\Sigma_{\text{pp}}^{(f)}(\mathbf{k}, \omega)$ in the particle-particle channel can be derived respectively in terms of the full hole diagonal and off-diagonal propagators as^{30,46},

$$\Sigma_{\text{ph}}^{(f)}(\mathbf{k}, i\omega_n) = \frac{t^2}{N} \sum_{\mathbf{p}} \frac{1}{\beta} \sum_{ip_m} G_f(\mathbf{p} + \mathbf{k}, ip_m + i\omega_n) \times P^{(0)}(\mathbf{k}, \mathbf{p}, ip_m), \quad (8a)$$

$$\Sigma_{\text{pp}}^{(f)}(\mathbf{k}, i\omega_n) = \frac{t^2}{N} \sum_{\mathbf{p}} \frac{1}{\beta} \sum_{ip_m} \mathfrak{S}_f^\dagger(\mathbf{p} + \mathbf{k}, ip_m + i\omega_n) \times P^{(0)}(\mathbf{k}, \mathbf{p}, ip_m), \quad (8b)$$

with the number of lattice sites N , the fermionic and bosonic Matsubara frequencies ω_n and p_m , respectively,

and the effective spin propagator $P^{(0)}(\mathbf{k}, \mathbf{p}, \omega)$, which depict the nature of the spin excitation, and can be derived as follows,

$$P^{(0)}(\mathbf{k}, \mathbf{p}, \omega) = \frac{1}{N} \sum_{\mathbf{q}} \Lambda_{\mathbf{p}+\mathbf{q}+\mathbf{k}}^2 \Pi(\mathbf{p}, \mathbf{q}, \omega), \quad (9)$$

where $\Lambda_{\mathbf{k}} = 4\gamma_{\mathbf{k}} - 4(t'/t)\gamma'_{\mathbf{k}}$ is the vertex function, while the spin bubble $\Pi(\mathbf{p}, \mathbf{q}, \omega)$ has been evaluated in terms of the spin propagator $D^{(0)-1}(\mathbf{q}, \omega) = [\omega^2 - \omega_{\mathbf{q}}^2]/B_{\mathbf{q}}$ as^{30,46},

$$\begin{aligned} \Pi(\mathbf{p}, \mathbf{q}, ip_m) &= \frac{1}{\beta} \sum_{iq_m} D^{(0)}(\mathbf{q}, iq_m) D^{(0)}(\mathbf{q} + \mathbf{p}, iq_m + ip_m) \\ &= -\frac{\bar{W}_{\mathbf{p}\mathbf{q}}^{(1)}}{(ip_m)^2 - [\omega_{\mathbf{p}\mathbf{q}}^{(1)}]^2} + \frac{\bar{W}_{\mathbf{p}\mathbf{q}}^{(2)}}{(ip_m)^2 - [\omega_{\mathbf{p}\mathbf{q}}^{(2)}]^2}, \end{aligned} \quad (10)$$

with the bosonic Matsubara frequencies p_m and q_m , $\omega_{\mathbf{p}\mathbf{q}}^{(1)} = \omega_{\mathbf{q}+\mathbf{p}} + \omega_{\mathbf{q}}$, $\omega_{\mathbf{p}\mathbf{q}}^{(2)} = \omega_{\mathbf{q}+\mathbf{p}} - \omega_{\mathbf{q}}$, and the functions,

$$\bar{W}_{\mathbf{p}\mathbf{q}}^{(1)} = \frac{B_{\mathbf{q}}B_{\mathbf{q}+\mathbf{p}}}{2\omega_{\mathbf{q}}\omega_{\mathbf{q}+\mathbf{p}}} \omega_{\mathbf{p}\mathbf{q}}^{(1)} [n_{\text{B}}(\omega_{\mathbf{q}+\mathbf{p}}) + n_{\text{B}}(\omega_{\mathbf{q}}) + 1], \quad (11a)$$

$$\bar{W}_{\mathbf{p}\mathbf{q}}^{(2)} = \frac{B_{\mathbf{q}}B_{\mathbf{q}+\mathbf{p}}}{2\omega_{\mathbf{q}}\omega_{\mathbf{q}+\mathbf{p}}} \omega_{\mathbf{p}\mathbf{q}}^{(2)} [n_{\text{B}}(\omega_{\mathbf{q}+\mathbf{p}}) - n_{\text{B}}(\omega_{\mathbf{q}})], \quad (11b)$$

where the spin excitation dispersion $\omega_{\mathbf{q}}$ and the weight function of the spin excitation spectrum $B_{\mathbf{q}}$ have been derived explicitly in Ref. 48, and then the effective spin propagator $P^{(0)}(\mathbf{k}, \mathbf{p}, \omega)$ in Eq. (9) is obtained directly from the above spin bubble in Eq. (10). Substituting the effective spin propagator in Eq. (9) into Eq. (8), the hole normal and anomalous self-energies $\Sigma_{\text{ph}}^{(f)}(\mathbf{k}, \omega)$ and $\Sigma_{\text{pp}}^{(f)}(\mathbf{k}, \omega)$ can be derived straightforwardly, and have been given explicitly in Ref. 46.

However, for the discussions of a link between the nature of the strange metallic normal-state and superconductivity in the overdoped electron-doped cuprate superconductors, we need to derive the full electron diagonal and off-diagonal propagators $G(\mathbf{k}, \omega)$ and $\mathfrak{S}^\dagger(\mathbf{k}, \omega)$, which are respectively associated with the hole diagonal and off-diagonal propagators $G_f(\mathbf{k}, \omega)$ and $\mathfrak{S}_f^\dagger(\mathbf{k}, \omega)$ in Eq. (6) via the particle-hole transformation $C_{l\sigma} \rightarrow f_{l-\sigma}^\dagger$ as $G(l-l', t-t') = \langle\langle C_{l\sigma}(t); C_{l'\sigma}^\dagger(t') \rangle\rangle = \langle\langle f_{l\sigma}^\dagger(t); f_{l'\sigma}(t') \rangle\rangle = -G_f(l-l', t-t')$ and $\mathfrak{S}(l-l', t-t') = \langle\langle C_{l\downarrow}(t); C_{l'\uparrow}(t') \rangle\rangle = \langle\langle f_{l\uparrow}^\dagger(t); f_{l'\downarrow}(t') \rangle\rangle = \mathfrak{S}_f^\dagger(l-l', t-t')$, and have been obtained explicitly as^{30,46},

$$G(\mathbf{k}, \omega) = \frac{1}{\omega - \varepsilon_{\mathbf{k}} - \Sigma_{\text{tot}}(\mathbf{k}, \omega)}, \quad (12a)$$

$$\mathfrak{S}^\dagger(\mathbf{k}, \omega) = \frac{L(\mathbf{k}, \omega)}{\omega - \varepsilon_{\mathbf{k}} - \Sigma_{\text{tot}}(\mathbf{k}, \omega)}, \quad (12b)$$

with the functions,

$$\Sigma_{\text{tot}}(\mathbf{k}, \omega) = \Sigma_{\text{ph}}(\mathbf{k}, \omega) + \frac{|\Sigma_{\text{pp}}(\mathbf{k}, \omega)|^2}{\omega + \varepsilon_{\mathbf{k}} + \Sigma_{\text{ph}}(\mathbf{k}, -\omega)}, \quad (13a)$$

$$L(\mathbf{k}, \omega) = -\frac{\Sigma_{\text{pp}}(\mathbf{k}, \omega)}{\omega + \varepsilon_{\mathbf{k}} + \Sigma_{\text{ph}}(\mathbf{k}, -\omega)}, \quad (13b)$$

where the electron non-interaction band energy $\varepsilon_{\mathbf{k}} = -\varepsilon_{\mathbf{k}}^{(f)} = -4t\gamma_{\mathbf{k}} + 4t'\gamma'_{\mathbf{k}} + \mu$, and the electron normal and anomalous self-energies are obtained as,

$$\Sigma_{\text{ph}}(\mathbf{k}, \omega) = -\Sigma_{\text{ph}}^{(f)}(\mathbf{k}, -\omega), \quad (14a)$$

$$\Sigma_{\text{pp}}(\mathbf{k}, \omega) = \Sigma_{\text{pp}}^{(f)}(\mathbf{k}, \omega). \quad (14b)$$

respectively. Moreover, the sharp peaks appear at low-temperature in $\Sigma_{\text{ph}}(\mathbf{k}, \omega)$, $\Sigma_{\text{pp}}(\mathbf{k}, \omega)$, and $P^{(0)}(\mathbf{k}, \mathbf{p}, \omega)$ are actually a δ -function that are broadened by a small damping employed in the numerical calculation for a finite lattice. As the approach described in Ref. 30, the calculation in this paper for $\Sigma_{\text{ph}}(\mathbf{k}, \omega)$, $\Sigma_{\text{pp}}(\mathbf{k}, \omega)$, and $P^{(0)}(\mathbf{k}, \mathbf{p}, \omega)$ is performed numerically on a 160×160 lattice in momentum space, where the infinitesimal $i0_+ \rightarrow i\Gamma$ is replaced by a small damping $\Gamma = 0.1J$.

C. Doping dependence of T_c

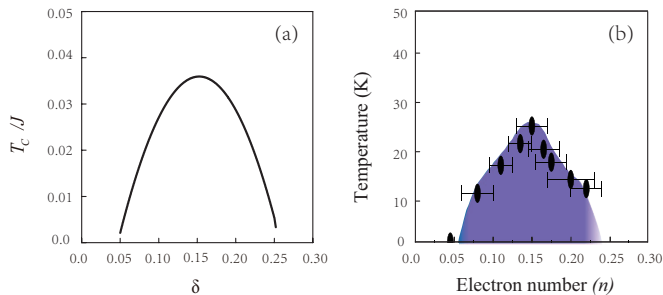


FIG. 1. (Color online) (a) Doping dependence of T_c . (b) The corresponding experimental result observed on $\text{Pr}_{1-x}\text{LaCe}_x\text{CuO}_{4-\delta}$ under the proper annealing condition taken from Ref. 9.

Based on the kinetic-energy-driven SC mechanism discussed in the above subsection IIB, the evolution of T_c with the electron doping in the electron-doped cuprate superconductors³⁰ has been investigated recently by making use of the self-consistent calculation in the condition of the SC gap $\tilde{\Delta}(\mathbf{k}) = \Sigma_{\text{pp}}(\mathbf{k}, 0) = 0$. For the convenience in the discussions of the correlation between the strength of the low-temperature T-linear normal-state resistivity and the corresponding magnitude of T_c in the overdoped electron-doped cuprate superconductors, the result of T_c as a function of the electron doping is replotted in Fig. 1a. For a better comparison, the corresponding experimental result⁹ observed on the electron-doped cuprate superconductor $\text{Pr}_{1-x}\text{LaCe}_x\text{CuO}_{4-\delta}$ under the proper annealing condition is also shown in Fig. 1b. Apparently, the experimental result⁹ of the doping dependent T_c in $\text{Pr}_{1-x}\text{LaCe}_x\text{CuO}_{4-\delta}$ under the proper annealing condition is qualitatively reproduced, where the gradual increase in T_c with the increase of the electron doping occurs in the underdoped regime, and T_c reaches its maximum at around the optimal electron doping $\delta \sim 0.15$, subsequently, T_c decreases monotonically

with the increase of the electron doping in the overdoped regime. In comparison with the corresponding result for the hole-doped case^{12,43}, it thus shows that although the magnitude of the optimized T_c in the electron-doped side is much lower than that in the hole-doped case, the doping range of the SC dome in the electron-doped side is in a striking analogy with that in the hole-doped case^{12,43}, which therefore confirms the absence of the disparity between the phase diagrams of the electron- and hole-doped cuprate superconductors⁸⁻¹².

D. Electron Fermi surface

The transition from the SC-state to the normal-state manifest in the anomalous self-energy (then the full electron off-diagonal propagator) becomes zero above T_c , and then the full electron propagator in Eq. (12) in the SC-state is reduced in the normal-state as,

$$G(\mathbf{k}, \omega) = \frac{1}{\omega - \varepsilon_{\mathbf{k}} - \Sigma_{\text{ph}}(\mathbf{k}, \omega)}, \quad (15)$$

while the electron spectrum function $A(\mathbf{k}, \omega) = -2\text{Im}G(\mathbf{k}, \omega)$ is obtained directly as,

$$A(\mathbf{k}, \omega) = \frac{-2\text{Im}\Sigma_{\text{ph}}(\mathbf{k}, \omega)}{[\omega - \varepsilon_{\mathbf{k}} - \text{Re}\Sigma_{\text{ph}}(\mathbf{k}, \omega)]^2 + [\text{Im}\Sigma_{\text{ph}}(\mathbf{k}, \omega)]^2}, \quad (16)$$

where $\text{Re}\Sigma_{\text{ph}}(\mathbf{k}, \omega)$ and $\text{Im}\Sigma_{\text{ph}}(\mathbf{k}, \omega)$ are the real and imaginary parts of the electron normal self-energy $\Sigma_{\text{ph}}(\mathbf{k}, \omega)$, respectively.

EFS separates the occupied and unoccupied states, and therefore the geometrical structure of EFS is closely linked with the low-energy electronic structure^{5,49-51} as well as the electrical transport⁵²⁻⁵⁴. In the recent work⁵⁵, the geometrical structure of EFS in the electron-doped cuprate superconductors has been studied, where the underlying EFS is obtained via the map of the electron spectral function (16) at zero energy $\omega = 0$, i.e., the closed EFS contour is determined by the poles of the full electron propagator (15) at zero energy: $\varepsilon_{\mathbf{k}} + \text{Re}\Sigma_{\text{ph}}(\mathbf{k}, 0) = \bar{\varepsilon}_{\mathbf{k}} = 0$, with the renormalized electron energy dispersion $\bar{\varepsilon}_{\mathbf{k}} = Z_F \varepsilon_{\mathbf{k}}$ and the single-particle coherent weight $Z_F^{-1} = 1 - \text{Re}\Sigma_{\text{pho}}(\mathbf{k}, 0) |_{\mathbf{k}=[\pi, 0]}$, while $\Sigma_{\text{pho}}(\mathbf{k}, \omega)$ that is the antisymmetric part of the electron normal self-energy $\Sigma_{\text{ph}}(\mathbf{k}, \omega)$. However, the strong redistribution of the spectral weight at the closed EFS contour is dominated by the the imaginary part of the electron normal self-energy $\text{Im}\Sigma_{\text{ph}}(\mathbf{k}, \omega)$ [then the single-particle scattering rate $\Gamma_{\mathbf{k}}(\omega) = -\text{Im}\Sigma_{\text{ph}}(\mathbf{k}, \omega)$]. To see this point more clearly, we plot the EFS map at the electron doping $\delta = 0.19$ with temperature $T = 0.002J$ in Fig. 2, where the Brillouin zone (BZ) center has been shifted by $[\pi, \pi]$, and AN, TFA, and ND indicate the antinode, tip of the Fermi arc, and node, respectively. Our result in Fig. 2 therefore shows that EFS has been separated into three typical regions due to the strong redistribution of the spectral weight⁵⁵: (i) the antinodal region, where the

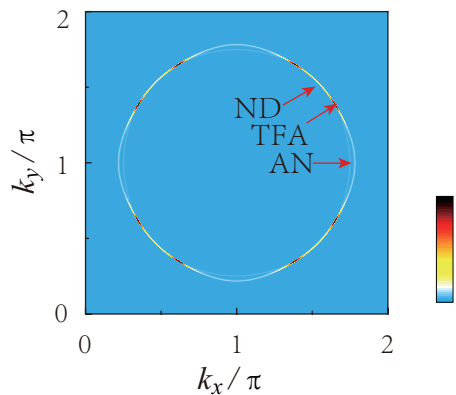


FIG. 2. (Color online) The map of the electron Fermi surface at $\delta = 0.19$ with $T = 0.002J$, where the Brillouin zone center has been shifted by $[\pi, \pi]$, and AN, TFA, and ND denote the antinode, tip of the Fermi arc, and node, respectively.

spectral weight is reduced strongly, leading to EFS at around the antinodal region to become invisible; (ii) the nodal region, where the spectral weight is reduced moderately, leading to EFS to be clearly visible as the reminiscence of the EFS contour in the case of the absence of the electron interaction to form the Fermi arcs; (iii) the region at around the tips of the Fermi arcs, where the dressing from the single-particle scattering further moves the spectral weight from the Fermi arcs to the tips of the Fermi arcs. As a result, the spectral weight exhibits the largest value at around the tips of the Fermi arcs. This EFS reconstruction is also qualitatively consistent with the recent experimental observations on the electron-doped cuprate superconductors^{8–11}, where upon the proper annealing, the weight of the ARPES spectrum around the antinodal region is reduced, and then EFS is truncated to form the Fermi arcs located around the nodal region.

E. Momentum relaxation in the normal-state

We now turn to discuss the normal-state electrical transport in the overdoped electron-doped cuprate superconductors. As in the hole-doped case^{49–51}, the conventional quasiparticle picture breaks down in the normal-state of the overdoped electron-doped cuprate superconductors⁵. In this case, two different methods have been employed to investigate the normal-state electrical transport in the case of the lack of the well-defined quasiparticle. The first one is the memory-matrix transport approach^{56–61}, which has a distinct advantage of not relying on the existence of the well-defined quasiparticle. In particular, the electrical transports in the strange-metal phases of different strongly correlated systems have been investigated based on the memory-matrix transport approach^{56–61}, and the obtained results are consistent with the corresponding experimental data. The another

method employed is the Boltzmann transport theory^{25,26}, where it is crucial to assume either the validity of the conventional quasiparticle picture or the treatment of the electron interaction mediated by different bosonic modes within the Eliashberg approach^{62,63}. This follows a basic fact that (i) in the early pioneering work⁶², Prange and Kadanoff have shown that in an electron-phonon system, a set of transport equations can be derived in the Migdal's approximation, where this coupled set of transport equations for the electron and phonon distribution functions is correct even in the case in which the electron excitation spectrum has considerable width and structure so that one might not expect a priori that there would be the well-defined quasiparticle⁶². Nevertheless, one of the forms of the electrical transport equation,

$$e\mathbf{E} \cdot \nabla_{\mathbf{k}} f(\mathbf{k}) = I_{e-e}, \quad (17)$$

is identical to the electrical transport equation proposed by Landau for the case of the existence of the well-defined quasiparticle^{25,26}, where e is the charge of an electron, $f(\mathbf{k}, t)$ is the distribution function in a homogeneous system, and for the convenience in the following discussions, the external magnetic field \mathbf{H} has been ignored, and only an external electric field \mathbf{E} is applied to the system, while I_{e-e} is the electron-electron collision term, and is directly related to the momentum relaxation mechanism; (ii) More importantly, it has been confirmed recently that this transport equation (17) developed by Prange and Kadanoff⁶² is not specific to a phonon-mediated interaction, and also is valid for the system with the interaction mediated by other bosonic excitations⁶³.

In the subsequent analysis, we investigate the low-temperature normal-state resistivity in the overdoped electron-doped cuprate superconductors based on the Boltzmann transport equation (17). To derive this Boltzmann transport equation (17), the linear perturbation from the equilibrium in terms of the distribution function,

$$f(\mathbf{k}) = n_{\text{F}}(\bar{\varepsilon}_{\mathbf{k}}) - \frac{dn_{\text{F}}(\bar{\varepsilon}_{\mathbf{k}})}{d\bar{\varepsilon}_{\mathbf{k}}} \tilde{\Phi}(\mathbf{k}), \quad (18)$$

can be introduced as it has been done in the previous works^{31,62,63}, where $\tilde{\Phi}(\mathbf{k})$ is a local shift of the chemical potential at a given patch of EFS^{31,62,63}, and obeys the antisymmetric relation $\tilde{\Phi}(-\mathbf{k}) = -\tilde{\Phi}(\mathbf{k})$. Substituting the above result in Eq. (18) into Eq. (17), we can linearize the Boltzmann equation (17) as,

$$e\mathbf{v}_{\mathbf{k}} \cdot \mathbf{E} \frac{\partial n_{\text{F}}(\bar{\varepsilon}_{\mathbf{k}})}{\partial \bar{\varepsilon}_{\mathbf{k}}} = I_{e-e}, \quad (19)$$

with the electron velocity $\mathbf{v}_{\mathbf{k}} = \nabla_{\mathbf{k}} \bar{\varepsilon}_{\mathbf{k}}$.

We now focus on the electron-electron collision term I_{e-e} , which is closely associated with the momentum relaxation mechanism^{25,26}. Although the momentum relaxation mechanism underlying the low-temperature T-linear resistivity in the strange metallic normal-state still remains controversial to date, it is likely of the electronic

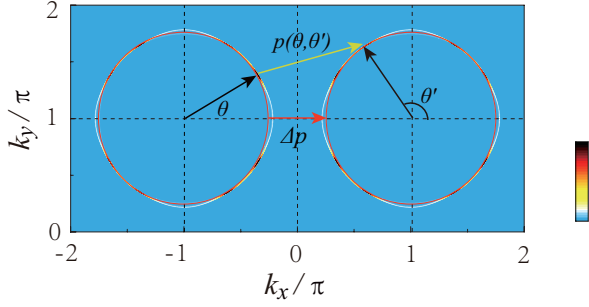


FIG. 3. (Color online) Schematic picture of the electron umklapp scattering process⁶³, where an electron on a electron Fermi surface (left) is scattered by its partner on the umklapp electron Fermi surface (right). The intensity map of the electron Fermi surface is the same as shown in Fig. 2, where the Fermi wave vector of the tips of the Fermi arcs k_F^{TFA} is the radius of the circular electron Fermi surface (red), and then an electron on this circular electron Fermi surface (left) parametrized by the Fermi angle θ is scattered to a point parametrized by the Fermi angle θ' on the umklapp electron Fermi surface (right) by the spin excitation carrying momentum $\mathbf{p}(\theta, \theta')$. Δ_p is the minimal umklapp vector at the antinode (the Fermi angle $\theta = 0$).

origin. In particular, it has been shown clearly that the electron umklapp scattering plays a crucial role in the normal-state transport of cuprate superconductors^{63–65}. In this paper, we employ the electron umklapp scattering to study the low-temperature normal-state resistivity in the overdoped electron-doped cuprate supercon-

ductors. To see this electron umklapp scattering process more clearly, a schematic picture of the electron umklapp scattering process⁶³ is shown in Fig. 3, where an electron on a circular EFS (left) is scattered by its partner on the umklapp EFS (right). The intensity map of EFS in Fig. 3 is identical to that shown in Fig. 2, where the Fermi wave vector of the tips of the Fermi arcs k_F^{TFA} is the radius of the circular EFS (red). This circle EFS (red) connects all tips of the Fermi arcs, and then almost all the fraction of the spectral weight is located on this circular EFS.

In the recent discussions⁶³, it has been shown that the electrical transport in the strange metallic normal-state of the overdoped hole-doped cuprate superconductors arises from the umklapp scattering between electrons by the exchange of a critical boson propagator, where the anisotropic transport scattering rate is T-linear in the low-temperature region near the umklapp point, which induces a low-temperature T-linear normal-state resistivity. Very recently, we³¹ have also studied the nature of the electrical transport in the strange metallic normal-state of the overdoped hole-doped cuprate superconductors, where the momentum dependence of the transport scattering rate originates from the umklapp scattering between electrons by the exchange of the effective spin propagator, and scales linearly with temperature in the low-temperature region, which then naturally generates a low-temperature T-linear normal-state resistivity. Following these recent discussions^{31,63}, the electron-electron collision I_{e-e} in Eq. (19) in the present case can be derived as,

$$I_{e-e} = \frac{1}{N^2} \sum_{\mathbf{k}', \mathbf{p}} \frac{2}{T} |P(\mathbf{k}, \mathbf{p}, \mathbf{k}', \bar{\epsilon}_{\mathbf{k}} - \bar{\epsilon}_{\mathbf{k}+\mathbf{p}+\mathbf{G}})|^2 \{ \tilde{\Phi}(\mathbf{k}) + \tilde{\Phi}(\mathbf{k}') - \tilde{\Phi}(\mathbf{k} + \mathbf{p} + \mathbf{G}) - \tilde{\Phi}(\mathbf{k}' - \mathbf{p}) \} \\ \times n_F(\bar{\epsilon}_{\mathbf{k}}) n_F(\bar{\epsilon}_{\mathbf{k}'})[1 - n_F(\bar{\epsilon}_{\mathbf{k}+\mathbf{p}+\mathbf{G}})][1 - n_F(\bar{\epsilon}_{\mathbf{k}'-\mathbf{p}})] \delta(\bar{\epsilon}_{\mathbf{k}} + \bar{\epsilon}_{\mathbf{k}'} - \bar{\epsilon}_{\mathbf{k}+\mathbf{p}+\mathbf{G}} - \bar{\epsilon}_{\mathbf{k}'-\mathbf{p}}), \quad (20)$$

where \mathbf{G} labels a set of reciprocal lattice vectors, and then the above electron umklapp scattering (20) is described as a scattering between electrons by the exchange of the effective spin propagator,

$$P(\mathbf{k}, \mathbf{p}, \mathbf{k}', \omega) = \frac{1}{N} \sum_{\mathbf{q}} \Lambda_{\mathbf{p}+\mathbf{q}+\mathbf{k}} \Lambda_{\mathbf{q}+\mathbf{k}'} \Pi(\mathbf{p}, \mathbf{q}, \omega), \quad (21)$$

rather than the scattering between electrons via the emission and absorption of the spin excitation³¹.

As in the hole-doped case⁶⁶, the electrons located at the bottom of the energy band (the deep inside EFS) in the electron-doped cuprate superconductors can not be thermally excited, and then all the low-temperature normal-state conduction processes involve only the low-energy electronic states at EFS. In this case, a given patch at the circular EFS shown in Fig. 3 is depicted via the Fermi angle θ with the angle range $\theta \in [0, 2\pi]$,

which leads to that the momentum integration along the perpendicular momentum is replaced by the integration over $\bar{\epsilon}_{\mathbf{k}}$ ^{62,63}. In the present case of the umklapp scattering between electrons by the exchange of the effective spin propagator, an electron on the circular EFS parametrized by the Fermi angle θ is scattered to a point parametrized by the Fermi angle θ' on the umklapp EFS in terms of the spin excitation carrying momentum $\mathbf{p}(\theta, \theta')$ as shown in Fig. 3. With the help of the above treatment, the electron-electron collision I_{e-e} in Eq. (20) can be derived straightforwardly, and has been given explicitly in Ref. 31. In this case, the Boltzmann transport equation (19) can be obtained as,

$$e \mathbf{v}_F(\theta) \cdot \mathbf{E} = -2 \int \frac{d\theta'}{2\pi} \zeta(\theta') F(\theta, \theta') [\Phi(\theta) - \Phi(\theta')], \quad (22)$$

with $\Phi(\theta) = \tilde{\Phi}[k(\theta)]$, the Fermi velocity $\mathbf{v}_F(\theta)$ at the Fermi angle θ , the density of states factor $\zeta(\theta') =$

$k_F^2/[4\pi^2v_F^3]$ at angle θ' , the Fermi wave vector k_F , and the Fermi velocity v_F , while the antisymmetric relation $\tilde{\Phi}(-\mathbf{k}) = -\tilde{\Phi}(\mathbf{k})$ for $\tilde{\Phi}(\mathbf{k})$ in Eq. (18) is replaced by the antisymmetric relation $\Phi(\theta) = -\Phi(\theta + \pi)$ for $\Phi(\theta)$ in the above Eq. (22). Moreover, the coefficient of $\Phi(\theta)$ in the first term of the right-hand side of Eq. (22),

$$\gamma(\theta) = 2 \int \frac{d\theta'}{2\pi} \zeta(\theta') F(\theta, \theta'), \quad (23)$$

is identified as the angular dependence of the transport scattering rate^{31,63}, where as shown in Fig. 3, the kernel function $F(\theta, \theta')$ links up the point θ on the circular EFS with the point θ' on the umklapp EFS via the magnitude of the momentum transfer $p(\theta, \theta')$, and can be expressed explicitly as,

$$F(\theta, \theta') = \frac{1}{T} \int \frac{d\omega}{2\pi} \frac{\omega^2}{p(\theta, \theta')} |\bar{P}[\mathbf{k}(\theta), p(\theta, \theta'), \omega]|^2 \times n_B(\omega)[1 + n_B(\omega)], \quad (24)$$

where the reduced effective spin propagator $\bar{P}[\mathbf{k}(\theta), p(\theta, \theta'), \omega]$ has been given explicitly in Ref. 31.

III. SCALING OF LOW-TEMPERATURE NORMAL-STATE TRANSPORT SCATTERING

The electron current density now can be derived via the local shift of the chemical potential $\Phi(\theta)$ as³¹,

$$\begin{aligned} \mathbf{J} &= en_0 \frac{1}{N} \sum_{\mathbf{k}} \mathbf{v}_{\mathbf{k}} \frac{dn_F(\bar{\epsilon}_{\mathbf{k}})}{d\bar{\epsilon}_{\mathbf{k}}} \tilde{\Phi}(\mathbf{k}) \\ &= -en_0 \frac{k_F}{v_F} \int \frac{d\theta}{(2\pi)^2} \mathbf{v}_F(\theta) \Phi(\theta), \end{aligned} \quad (25)$$

where the momentum relaxation is induced by the action of the electric field on the mobile electrons⁶⁶ at EFS with the density n_0 . In particular, the local shift of the chemical potential $\Phi(\theta)$ can be obtained in the relaxation-time approximation as^{31,63}, $\Phi(\theta) = -ev_F \cos(\theta) E_{\hat{x}}/[2\gamma(\theta)]$, with the electric field \mathbf{E} that has been chosen along the \hat{x} -axis. In this case, the dc conductivity can be obtained straightforwardly as^{31,63},

$$\sigma_{dc}(T) = \frac{1}{2} e^2 n_0 k_F v_F \int \frac{d\theta}{(2\pi)^2} \cos^2(\theta) \frac{1}{\gamma(\theta)}, \quad (26)$$

while the normal-state resistivity is related directly to the above dc conductivity, and can be expressed explicitly as,

$$\rho(T) = \frac{1}{\sigma_{dc}(T)}, \quad (27)$$

which therefore shows that the electron-electron collision I_{e-e} (20) originated from the umklapp scattering between electrons by the exchange of the effective spin propagator leads to the appearance of the electrical resistance.

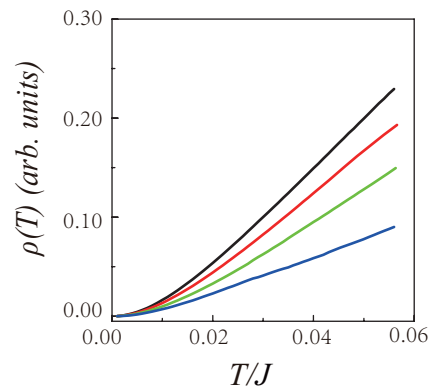


FIG. 4. (Color online) The normal-state resistivity as a function of temperature at $\delta = 0.15$ (black-line), $\delta = 0.17$ (red-line), $\delta = 0.19$ (green-line), and $\delta = 0.21$ (blue-line).

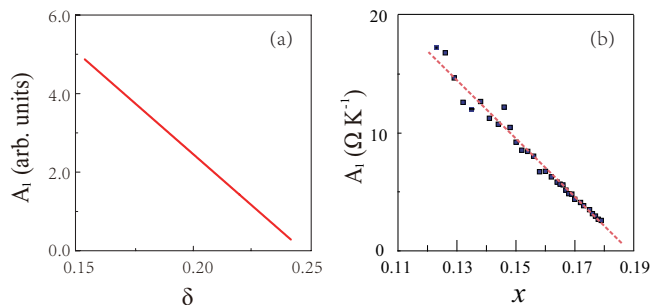


FIG. 5. (a) The strength of the low-temperature T-linear normal-state resistivity as a function of doping. (b) The corresponding experimental result of $\text{La}_{2-x}\text{Ce}_x\text{CuO}_4$ taken from Ref. 23.

In Fig. 4, we plot the normal-state resistivity $\rho(T)$ in Eq. (27) as a function of temperature at the electron doping concentrations $\delta = 0.15$ (black-line), $\delta = 0.17$ (red-line), $\delta = 0.19$ (green-line), and $\delta = 0.21$ (blue-line), where the temperature region is clearly divided into two characteristic regions: (i) the low-temperature region ($T > 0.01J \approx 10\text{K}$), where the normal-state resistivity $\rho(T)$ is T-linear over a wide range of electron doping concentrations in the overdoped regime, with the strength of the T-linear normal-state resistivity (then the T-linear normal-state resistivity coefficient) A_1 that rises with the electron doping concentration as the electron doping concentration decreases from the edge of the SC dome, in qualitative agreement with the corresponding experimental results^{17–23}. To see this evolution of the T-linear resistivity strength A_1 with the electron doping concentration more clearly, we plot A_1 as a function of the electron doping in Fig. 5a. For a better comparison, the corresponding experimental result²³ observed on the electron-doped cuprate superconductor $\text{La}_{2-x}\text{Ce}_x\text{CuO}_4$ in the overdoped regime is also shown in Fig. 5b. The obtained result thus shows that A_1 decreases linearly with the increase of the electron doping concentration for the overdoping up to the edge of the SC dome,

also in qualitative agreement with the corresponding experimental data^{17–23}; (ii) the far-lower-temperature region ($T < 0.01J \approx 10\text{K}$), where a departure from its low-temperature T-linear behaviour occurs, developing a nonlinear behaviour in the far-lower-temperature region. To see this nonlinear behaviour more clearly, we have fitted the present result of the normal-state resistivity $\rho(T)$ in the far-lower-temperature region, and found that in the far-lower-temperature region, the normal-state resistivity decreases quadratically with the decrease of temperature.

In addition to the above results of the low-temperature T-linear normal-state resistivity, we have also performed a numerical calculation for the transport scattering rate $\gamma(\theta)$ in Eq. (23), and the obtained results show that the overall feature of the strong angular dependence of $\gamma(\theta)$ in the electron-doped side is quite similar to the corresponding one in the hole-doped case³¹, where $\gamma(\theta)$ has the largest value at around the antinodal region, and then it decreases with the move of the Fermi angle away from the antinode. In particular, although the magnitude of $\gamma(\theta)$ at around the nodal region is smaller than that at around the antinodal region, $\gamma(\theta)$ exhibits its minimum at around the tips of the Fermi arcs, which therefore show that the normal-state transport is mainly governed by $\gamma(\theta)$ at both the antinodal and nodal regions. Moreover, also as in the hole-doped case³¹, although both the strengths of the nodal and antinodal umklapp scattering decrease as the temperature is decreased, the decrease of the strength of the nodal umklapp scattering is slower than that of the antinodal umklapp scattering, leading to a tendency with the antinodal umklapp scattering that tends to generate the T-linear normal-state resistivity, while the nodal umklapp scattering that tends to induce a departure from the T-linear normal-state resistivity. The current findings together with our recent work for the hole-doped case³¹ therefore also show that the low-temperature T-linear normal-state resistivity in the overdoped electron-doped cuprate superconductors is of the same origin as the low-temperature T-linear normal-state resistivity in the overdoped hole-doped cuprate superconductors.

We now turn to discuss the intrinsic correlation between the strength of the low-temperature T-linear normal-state resistivity and the corresponding magnitude of T_c in the overdoped electron-doped cuprate superconductors. In Fig. 6a, we plot the square-root of the strength of the low-temperature T-linear normal-state resistivity $\sqrt{A_1}$ as a function of T_c . For a clear comparison, the corresponding experimental result²³ observed on $\text{La}_{2-x}\text{Ce}_x\text{CuO}_4$ in the overdoped regime is also shown in Fig. 6b. It thus shows clearly in Fig. 6 that the experimental result²³ of the scaling relation between the strength of the low-temperature T-linear normal-state resistivity $\sqrt{A_1}$ and the corresponding magnitude of T_c in the overdoped electron-doped cuprate superconductors is qualitatively reproduced, where $\sqrt{A_1}/\sqrt{A_1^{\text{max}}}$ is grown linearly when T_c/T_c^{max} is raised, with A_1^{max} and T_c^{max}

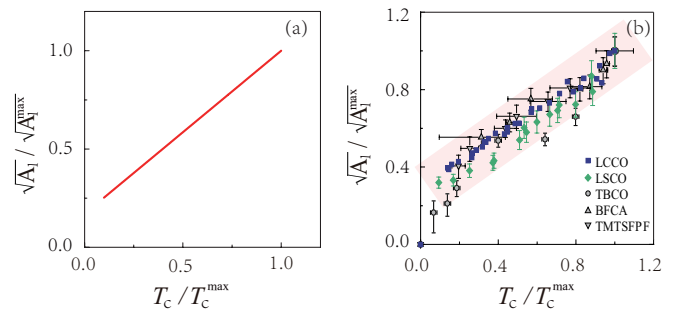


FIG. 6. (a) The correlation between the square-root of the T-linear normal-state resistivity strength $\sqrt{A_1}/\sqrt{A_1^{\text{max}}}$ and the corresponding magnitude of T_c/T_c^{max} , where A_1^{max} and T_c^{max} are maximal values of the T-linear normal-state resistivity strength and superconducting transition temperature at the optimal electron doping, respectively. (b) The corresponding experimental result of $\text{La}_{2-x}\text{Ce}_x\text{CuO}_4$ taken from Ref. 23.

that are maximal values of the strength of the T-linear normal-state resistivity and SC transition temperature at the optimal electron doping, respectively. In other words, the evolution of T_c correlates with the emergence of the low-temperature T-linear normal-state resistivity in the overdoped regime, and then the magnitude of $\sqrt{A_1}$ decreases as T_c decreases. The present result of the scaling relation in Fig. 6 therefore also confirms the intimate connection between the nature of the strange metallic normal-state and superconductivity observed on the overdoped electron-doped cuprate superconductors^{17–23}.

The essential physics of the crossover from the T-linear normal-state resistivity in the low-temperature region into T-quadratic normal-state resistivity in the far-lower-temperature region invoked for the overdoped hole-doped case³¹ straightforwardly applies here on the overdoped electron-doped side, and is attributed to the electron umklapp scattering mediated by the *spin excitation*. The nature of the transport scattering rate in Eq. (23) [then the nature of the normal-state resistivity in Eq. (27)] is dominated by the nature of the kernel function $F(\theta, \theta')$ in Eq. (24), while this kernel function $F(\theta, \theta')$ is proportional to the effective spin propagator $P(\mathbf{k}, \mathbf{p}, \mathbf{k}', \omega)$ in Eq. (21), which can be expressed more clearly as,

$$P(\mathbf{k}, \mathbf{p}, \mathbf{k}', \omega) = -\frac{1}{N} \sum_{\mathbf{q}} \left[\frac{\varpi_1(\mathbf{k}, \mathbf{p}, \mathbf{k}', \mathbf{q})}{\omega^2 - [\omega_{\mathbf{p}\mathbf{q}}^{(1)}]^2} - \frac{\varpi_2(\mathbf{k}, \mathbf{p}, \mathbf{k}', \mathbf{q})}{\omega^2 - [\omega_{\mathbf{p}\mathbf{q}}^{(2)}]^2} \right], \quad (28)$$

with the functions,

$$\varpi_1(\mathbf{k}, \mathbf{p}, \mathbf{k}', \mathbf{q}) = \Lambda_{\mathbf{k}+\mathbf{p}+\mathbf{q}} \Lambda_{\mathbf{q}+\mathbf{k}'} \bar{W}_{\mathbf{p}\mathbf{q}}^{(1)}, \quad (29a)$$

$$\varpi_2(\mathbf{k}, \mathbf{p}, \mathbf{k}', \mathbf{q}) = \Lambda_{\mathbf{k}+\mathbf{p}+\mathbf{q}} \Lambda_{\mathbf{q}+\mathbf{k}'} \bar{W}_{\mathbf{p}\mathbf{q}}^{(2)}. \quad (29b)$$

Following the recent discussions for the hole-doped case³¹, we can also make a Taylor expansion for the effective spin excitation energy dispersions $\omega_{\mathbf{p}\mathbf{q}}^{(1)}$ and $\omega_{\mathbf{p}\mathbf{q}}^{(2)}$ in

the electron-doped side, and then the effective spin excitation energy dispersions $\omega_{\mathbf{p}\mathbf{q}}^{(1)}$ and $\omega_{\mathbf{p}\mathbf{q}}^{(2)}$ can be obtained approximately as,

$$\omega_{\mathbf{p}\mathbf{q}}^{(1)} = \omega_{\mathbf{q}+\mathbf{p}} + \omega_{\mathbf{q}} \approx a(\mathbf{q})p^2 + 2\omega_{\mathbf{q}}, \quad (30a)$$

$$\omega_{\mathbf{p}\mathbf{q}}^{(2)} = \omega_{\mathbf{q}+\mathbf{p}} - \omega_{\mathbf{q}} \approx a(\mathbf{q})p^2, \quad (30b)$$

with $a(\mathbf{q}) = (d^2\omega_{\mathbf{q}}/d^2\mathbf{q})$. The above results in Eq. (30) show that the effective spin propagator $P(\mathbf{k}, \mathbf{p}, \mathbf{k}', \omega)$ in Eq. (28) scales with p^2 . Moreover, when the electron umklapp scattering kicks in, the temperature scale that is proportional to Δ_p^2 can be very low^{31,63} due to the presence of this p^2 scaling in the effective spin propagator (28). In this case, $T_{\text{scale}} = \bar{a}\Delta_p^2$ can be identified as the temperature scale, with the average value $\bar{a} = (1/N)\sum_{\mathbf{q}} a(\mathbf{q})$ that is a constant at a given electron doping. In particular, our numerical result indicates that the temperature scale $T_{\text{scale}} = \bar{a}\Delta_p^2 = 0.01247J \approx 12\text{K}$ at the electron doping concentration $\delta = 0.19$, also in good agreement with the crossover temperature shown in Fig. 4.

According to the above temperature scale T_{scale} , we now follows the analyses carried out in the hole-doped case³¹ to show that the temperature region in the electron-doped side shown in Fig. 4 can also be divided into three characteristic regions:

(i) the low-temperature region, where $T > T_{\text{scale}} + \omega_{\mathbf{k}_A}$ with the spin excitation energy $\omega_{\mathbf{k}_A} \approx 0.0022J \sim 2\text{K}$ at the $[\pi, \pi]$ point of BZ. In this low-temperature region, the kernel function $F(\theta, \theta')$ can be reduced as $F(\theta, \theta') \propto T$, which generates a low-temperature T-linear normal-state resistivity $\rho(T) \propto T$ as shown in Fig. 4;

(ii) the far-lower-temperature region, where $T < T_{\text{scale}}$. In this far-lower-temperature region, the kernel function $F(\theta, \theta')$ can be reduced as $F(\theta, \theta') \propto T^2$, which leads to a T-quadratic normal-state resistivity $\rho(T) \propto T^2$ as shown in Fig. 4;

(iii) the crossover temperature region, where $T_{\text{scale}} < T < T_{\text{scale}} + \omega_{\mathbf{k}_A}$. In this extremely narrow crossover temperature region, the normal-state resistivity does not exhibit a T-linear or a T-quadratic behavior, but instead shows a nonlinear behavior with respect to temperature.

We now turn to show why the strength of the low-temperature T-linear normal-state resistivity correlates with the corresponding magnitude of T_c in the overdoped electron-doped cuprate superconductors to form the scaling relation shown Fig. 6: (i) in the framework of the kinetic-energy-driven superconductivity^{40–43}, the main ingredient is identified into an electron pairing mechanism involving *the spin excitation*, where both the electron pair gap (then the anomalous self-energy in the particle-particle channel) and the single-particle coherence (then the normal self-energy in the particle-hole channel) arise from the interaction between electrons mediated by *the spin excitation*, and then the SC-state is controlled by both the electron pair gap and the single-particle coherence, which leads to that the maximal T_c occurs around the optimal electron doping, and

then decreases in both the underdoped and the overdoped regimes as shown in Fig. 1; (ii) on the other hand, the results presented here show that the low-temperature T-linear normal-state resistivity in the overdoped regime shown in Fig. 4 arises from the momentum relaxation due to the electron umklapp scattering mediated by *the same spin excitation*, and then the strength of the low-temperature T-linear normal-state resistivity decreases as T_c decreases as shown in Fig. 5. In other words, this *same spin excitation* that mediates both the pairing electrons responsible for superconductivity and the electron umklapp scattering responsible for the low-temperature T-linear normal-state resistivity induces a correlation between the strength of the low-temperature T-linear normal-state resistivity and the corresponding magnitude of T_c in the overdoped electron-doped cuprate superconductors as shown in Fig. 6.

IV. SUMMARY

Within the framework of the kinetic-energy-driven superconductivity, we have rederived the doping dependence of T_c in the electron-doped cuprate superconductors, where the glue to hold the constrained electron pairs together is *the spin excitation, the collective mode from the internal spin degree of freedom of the constrained electron itself*, then T_c achieves its maximum at around the optimal electron doping, and decreases in both the underdoped and overdoped regimes. By virtue of this doping dependence of T_c , we then have investigated the correlation between the strength of the low-temperature T-linear normal-state resistivity and the corresponding magnitude of T_c in the overdoped electron-doped cuprate superconductors, where the low-temperature T-linear normal-state resistivity in the overdoped regime arises from the momentum relaxation due to the electron umklapp scattering mediated by *the same spin excitation*. The result of the low-temperature T-linear normal-state resistivity in this paper together with the previous work for superconductivity³⁰ therefore identify explicitly that the *spin excitation* is at the origin of both the low-temperature T-linear normal-state resistivity and superconductivity. This *same spin excitation* therefore leads to that the strength of the low-temperature T-linear normal-state resistivity well tracks the corresponding magnitude of T_c in the overdoped electron-doped cuprate superconductors.

ACKNOWLEDGEMENTS

XM, MZ, and SP are supported by the National Key Research and Development Program of China under Grant No. 2021YFA1401803, and the National Natural Science Foundation of China under Grant Nos. 11974051, 12274036, and 12247116. HG acknowledges support from the National Natural Science Foundation of China under

- * spfeng@bnu.edu.cn
- ¹ See, e.g., the review, M. Fujita, H. Hiraka, M. Matsuda, M. Matsuura, J. M. Tranquada, S. Wakimoto, G. Xu, and K. Yamada, *J. Phys. Soc. Jpan.* **81**, 011007 (2012).
 - ² P. W. Anderson, *Science* **235**, 1196 (1987).
 - ³ J. G. Bednorz and K. A. Müller, *Z. Phys. B* **64**, 189 (1986).
 - ⁴ Y. Tokura, H. Takagi, and S. Uchida, *Nature* **337**, 345 (1989).
 - ⁵ See, e.g., the review, N. P. Armitage, P. Fournier, and R. L. Greene, *Rev. Mod. Phys.* **82**, 2421 (2010).
 - ⁶ T. Adachi, Y. Mori, A. Takahashi, M. Kato, T. Nishizaki, T. Sasaki, N. Kobayashi, and Y. Koike, *J. Phys. Soc. Jpn.* **82**, 063713 (2013).
 - ⁷ See, e.g., the review, T. Adachi, T. Kawamata, Y. Koike, *Condensed Matter* **2**, 23 (2017).
 - ⁸ M. Horio, T. Adachi, Y. Mori, A. Takahashi, T. Yoshida, H. Suzuki, L. C. C. Ambolode II, K. Okazaki, K. Ono, H. Kumigashira, H. Anzai, M. Arita, H. Namatame, M. Taniguchi, D. Ootsuki, K. Sawada, M. Takahashi, T. Mizokawa, Y. Koike and A. Fujimori, *Nat. Commun.* **7**, 10567 (2016).
 - ⁹ D. Song, G. Han, W. Kyung, J. Seo, S. Cho, B. S. Kim, M. Arita, K. Shimada, H. Namatame, M. Taniguchi, Y. Yoshida, H. Eisaki, S. R. Park, and C. Kim, *Phys. Rev. Lett.* **118**, 137001 (2017).
 - ¹⁰ C. Lin, T. Adachi, M. Horio, T. Ohgi, M.A. Baqiya, T. Kawamata, H. Sato, T. Sumura, K. Koshiishi, S. Nakata, G. Shibata, K. Hagiwara, M. Suzuki, K. Ono, K. Horiba, H. Kumigashira, S. Ideta, K. Tanaka, Y. Koike, A. Fujimori, arXiv:2006.04524.
 - ¹¹ M. Horio, K. P. Kramer, Q. Wang, A. Zaidan, K. von Arx, D. Sutter, C. E. Matt, Y. Sassa, N. C. Plumb, M. Shi, A. Hanff, S. K. Mahatha, H. Bentmann, F. Reinert, S. Rohlf, F. K. Diekmann, J. Buck, M. Kalläne, K. Rosnagel, E. Rienks, V. Granata, R. Fittipaldi, A. Vecchione, T. Ohgi, T. Kawamata, T. Adachi, Y. Koike, A. Fujimori, M. Hoesch, *J. Chang, Phys. Rev. B* **102**, 245153 (2020).
 - ¹² I. K. Drozdov, I. Pletikosić, C. -K. Kim, K. Fujita, G. D. Gu, J. C. S. Davis, P. D. Johnson, I. Božović, and T. Valla, *Nat. Commun.* **9**, 5210 (2018).
 - ¹³ See, e.g., the review, L. Taillefer, *Annu. Rev. Condens. Matter Phys.* **1**, 51 (2010).
 - ¹⁴ P. Li, F. F. Balakirev, and R. L. Greene, *Phys. Rev. Lett.* **99**, 047003 (2007).
 - ¹⁵ N. R. Poniatowski, T. Sarkar, and R. L. Greene, *Phys. Rev. B* **103**, 125102 (2021).
 - ¹⁶ N. R. Poniatowski, T. Sarkar, S. D. Sarma, and R. L. Greene, *Phys. Rev. B* **103**, L020501 (2021).
 - ¹⁷ See, e.g., the review, R. L. Greene, P. R. Mandal, N. R. Poniatowski, and T. Sarkar, *Annu. Rev. Condens. Matter Phys.* **11**, 213 (2020).
 - ¹⁸ P. Fournier, P. Mohanty, E. Maiser, S. Darzens, T. Venkatesan, C. J. Lobb, G. Czjzek, R. A. Webb, and R. L. Greene, *Phys. Rev. Lett.* **81**, 4720 (1998).
 - ¹⁹ K. Jin, N. P. Butch, K. Kirshenbaum, J. Paglione, and R. L. Greene, *Nature* **476**, 73 (2011).
 - ²⁰ T. Sarkar, P. R. Mandal, J. S. Higgins, Y. Zhao, H. Yu, K. Jin, and R. L. Greene, *Phys. Rev. B* **96**, 155449 (2017).
 - ²¹ T. Sarkar, P. R. Mandal, N. R. Poniatowski, M. K. Chan, R. L. Greene, *Sci. Adv.* **5**, eaav6753 (2019).
 - ²² A. Legros, S. Benhabib, W. Tabis, F. Laliberté, M. Dion, M. Lizaire, B. Vignolle, D. Vignolles, H. Raffy, Z. Z. Li, P. Auban-Senzier, N. Doiron-Leyraud, P. Fournier, D. Colson, L. Taillefer, and C. Proust, *Nat. Phys.* **15**, 142 (2019).
 - ²³ J. Yuan, Q. Chen, K. Jiang, Z. Feng, Z. Lin, H. Yu, G. He, J. Zhang, X. Jiang, X. Zhang, Y. Shi, Y. Zhang, M. Qin, Z. Cheng, N. Tamura, Y.-F. Yang, T. Xiang, J. Hu, I. Takeuchi, K. Jin, and Z. Zhao, *Nature* **602**, 431 (2022).
 - ²⁴ See, e.g., J. R. Schrieffer, *Theory of Superconductivity*, Benjamin, New York, 1964.
 - ²⁵ See, e.g., A. A. Abrikosov, *Fundamentals of the Theory of Metals*, Elsevier Science Publishers B. V., 1988.
 - ²⁶ See, e.g., G. D. Mahan, *Many-Particle Physics*, (Plenum Press, New York, 1981).
 - ²⁷ See, e.g., the review, B. Keimer, S. A. Kivelson, M. R. Norman, S. Uchida, and J. Zaanen, *Nature* **518**, 179 (2015).
 - ²⁸ See, e.g., the review, C. M. Varma, *Rev. Mod. Phys.* **92**, 031001 (2020).
 - ²⁹ P. W. Phillips, N. E. Hussey, and P. Abbamonte, *Science* **377**, 169 (2022).
 - ³⁰ S. Tan, Y. Liu, Y. Mou, and S. Feng, *Phys. Rev. B* **103**, 014503 (2021).
 - ³¹ X. Ma, M. Zeng, Z. Cao, and S. Feng, *Phys. Rev. B* **108**, 134502 (2023).
 - ³² Mark S. Hybertsen, E. B. Stechel, M. Schluter, and D. R. Jennison, *Phys. Rev. B* **41**, 11068 (1990).
 - ³³ R. J. Gooding, K. J. E. Vos, and P. W. Leung, *Phys. Rev. B* **50**, 12866 (1994).
 - ³⁴ C. Kim, P. J. White, Z.-X. Shen, T. Tohyama, Y. Shibata, S. Maekawa, B. O. Wells, Y. J. Kim, R. J. Birgeneau, and M. A. Kastner, *Phys. Rev. Lett.* **80**, 4245 (1998).
 - ³⁵ See, e.g., the review, L. Yu, Many-body problems in high temperature superconductors, in *Recent Progress in Many-Body Theories*, edited by T. L. Ainsworth, C. E. Campbell, B. E. Clements, and E. Krotscheck (Plenum, New York, 1992), Vol. **3**, p. 157.
 - ³⁶ S. Feng, J.B. Wu, Z.B. Su, and L. Yu, *Phys. Rev. B* **47**, 15192 (1993).
 - ³⁷ L. Zhang, J. K. Jain, and V. J. Emery, *Phys. Rev. B* **47**, 3368 (1993).
 - ³⁸ See, e.g., the review, P. A. Lee, N. Nagaosa, and X.-G. Wen, *Rev. Mod. Phys.* **78**, 17 (2006).
 - ³⁹ S. Feng, J. Qin, and T. Ma, *J. Phys.: Condens. Matter* **16**, 343 (2004); S. Feng, Z. B. Su, and L. Yu, *Phys. Rev. B* **49**, 2368 (1994).
 - ⁴⁰ See, e.g., the review, S. Feng, Y. Lan, H. Zhao, L. Kuang, L. Qin, and X. Ma, *Int. J. Mod. Phys. B* **29**, 1530009 (2015).
 - ⁴¹ S. Feng, *Phys. Rev. B* **68**, 184501 (2003); S. Feng, T. Ma, and H. Guo, *Physica C* **436**, 14 (2006).
 - ⁴² S. Feng, H. Zhao, and Z. Huang, *Phys. Rev. B* **85**, 054509 (2012); *Phys. Rev. B* **85**, 099902(E) (2012).
 - ⁴³ S. Feng, L. Kuang, and H. Zhao, *Physica C* **517**, 5 (2015).
 - ⁴⁴ J. R. Schrieffer, *J. Low Temp. Phys.* **99**, 397 (1995).
 - ⁴⁵ K.-J. Xu, Q. Guo, M. Hashimoto, Z.-X. Li, S.-D. Chen, J. He, Y. He, C. Li, M. H. Berntsen, C. R.

- Rotundu, Y. S. Lee, T. P. Devereaux, A. Rydh, D.-H. Lu, D.-H. Lee, O. Tjernberg, Z.-X. Shen, *Nature Phys.* (2023). <https://doi.org/10.1038/s41567-023-02209-x>. arXiv:2308.05313.
- ⁴⁶ S. Tan, Y. Mou, Y. Liu, and S. Feng, *J. Supercond. Nov. Magn.* **33**, 2305 (2020).
- ⁴⁷ G. M. Eliashberg, *Sov. Phys. JETP* **11**, 696 (1960).
- ⁴⁸ L. Cheng and S. Feng, *Phys. Rev B* **77**, 054518 (2008).
- ⁴⁹ See, e.g., the review, J. C. Campuzano, M. R. Norman, M. Randeria, in *Physics of Superconductors*, vol. II, edited by K. H. Bennemann and J. B. Ketterson (Springer, Berlin Heidelberg New York, 2004), p. 167.
- ⁵⁰ See, e.g., the review, A. Damascelli, Z. Hussain, and Z.-X. Shen, *Rev. Mod. Phys.* **75**, 473 (2003).
- ⁵¹ See, e.g., the review, J. Fink, S. Borisenko, A. Kordyuk, A. Koitzsch, J. Geck, V. Zabalotnyy, M. Knupfer, B. Buechner, and H. Berger, in *Lecture Notes in Physics*, vol. 715, edited by S. Hüfner (Springer-Verlag Berlin Heidelberg, 2007), p. 295.
- ⁵² See, e.g., the review, N. E. Hussey, *J. Phys.: Condens. Matter* **20**, 123201 (2008).
- ⁵³ See, e.g., the review, T. Timusk and B. Statt, *Rep. Prog. Phys.* **62**, 61 (1999).
- ⁵⁴ See, e.g., the review, M. A. Kastner, R. J. Birgeneau, G. Shirane, and Y. Endoh, *Magnetic, Rev. Mod. Phys.* **70**, 897 (1998).
- ⁵⁵ Y. Mou and S. Feng, *Phil. Mag.* **97**, 3361 (2017).
- ⁵⁶ R. Mahajan, M. Barkeshli, and S. A. Hartnoll, *Phys. Rev. B* **88**, 125107 (2013).
- ⁵⁷ S. A. Hartnoll, R. Mahajan, M. Punk, and S. Sachdev, *Phys. Rev. B* **89**, 155130 (2014).
- ⁵⁸ A. A. Patel and S. Sachdev, *Phys. Rev. B* **90**, 165146 (2014).
- ⁵⁹ A. Lucas and S. Sachdev, *Phys. Rev. B* **91**, 195122 (2015).
- ⁶⁰ L. E. Vieira, V. S. de Carvalho, H. Freire, *Ann. Phys.* **419**, 168230 (2020).
- ⁶¹ I. Mandal and H. Freire, *Phys. Rev. B* **103**, 195116 (2021).
- ⁶² R. E. Prange and L. P. Kadanoff, *Phys. Rev.* **134**, A566 (1964).
- ⁶³ P. A. Lee, *Phys. Rev. B* **104**, 035140 (2021).
- ⁶⁴ T. M. Rice, N. J. Robinson, and A. M. Tsvelik, *Phys. Rev. B* **96**, 220502(R) (2017).
- ⁶⁵ N. E. Hussey, *Eur. Phys. J. B* **31**, 495 (2003).
- ⁶⁶ F. D. M. Haldane, arXiv:1811.12